Observation of a super-tetrahedral cluster of acetonitrile-solvated dodecaborate dianion via dihydrogen bonding

Xiaogai Peng[1#], Wenjin Cao[2#], Zhubin Hu[1#], Yan Yang[1], Zhenrong Sun[1],

Xue-Bin Wang[2,*], and Haitao Sun[1,3,4,*]

[1] *State Key Laboratory of Precision Spectroscopy,*

School of Physics and Electronic Science,

East China Normal University, Shanghai 200241, China

[2] *Physical Sciences Division, Pacific Northwest National Laboratory,*

902 Battelle Boulevard, P.O. Box 999, Richland, Washington 99352, USA

[3]*Collaborative Innovation Center of Extreme Optics, Shanxi University,*

Taiyuan, Shanxi 030006, China

[4]*NYU-ECNU Center for Computational Chemistry at NYU Shanghai, Shanghai,*

200062, China

[#]X. Peng, W. Cao, and Z. Hu contributed equally to this work.

*Corresponding author: htsun@phy.ecnu.edu.cn (H.S.); xuebin.wang@pnnl.gov (X.-B.W.).

ABSTRACT

We launched a combined negative ion photoelectron spectroscopy (NIPES) and multiscale theoretical investigation on the geometric and electronic structures of a series of acetonitrile-solvated dodecaborate clusters, *i.e.* $B_{12}H_{12}^{2-}\cdot n CH_3CN$ (n = 1–4). The electron binding energies (EBEs) of $B_{12}H_{12}^{2-}\cdot n CH_3CN$ are observed to increase with cluster size suggesting their enhanced electronic stability. B3LYP-D3(BJ)/ma-def2-TZVP geometry optimizations indicate each acetonitrile molecule binds to $B_{12}H_{12}^{2-}$ via a threefold dihydrogen bond (DHB) B3–H3 ⋮⋮ H3C–CN unit, in which three adjacent nucleophilic H atoms in $B_{12}H_{12}^{2-}$ interact with the three methyl hydrogens of acetonitrile. The structural evolution from n = 1 to 4 can be rationalized by the surface charge redistributions through the restrained electrostatic potential (RESP) analysis. Notably, a super-tetrahedral cluster of $B_{12}H_{12}^{2-}$ solvated by four acetonitrile molecules with twelve DHBs is observed. The post-Hartree-Fock DLPNO-CCSD(T) calculated vertical detachment energies (VDEs) agree well with the experimental measurements, confirming the identified isomers as the most stable ones. Further, the nature and strength of the intermolecular interactions between $B_{12}H_{12}^{2-}$ and CH_3CN are revealed by the quantum theory of atoms-in-molecules (QTAIM) and the energy decomposition analysis. Ab initio molecular dynamics (AIMD) simulations are conducted at various temperatures to reveal the great kinetic and thermodynamic stabilities of the selected $B_{12}H_{12}^{2-}\cdot CH_3CN$ cluster. The binding motif in $B_{12}H_{12}^{2-}\cdot CH_3CN$ is largely retained for the whole halogenated series $B_{12}X_{12}^{2-}\cdot CH_3CN$ (X = F – I). This study provides a molecular-level understanding of structural evolution for acetonitrile-solvated dodecaborate clusters and a fresh view by examining acetonitrile as a real HB donor to form strong HB interactions.

I. INTRODUCTION

Specific-ion solvation effect has been known for more than 130 years since Lewith and Hofmeister's pioneering work.[1-3] It has been related to the widespread concepts such as Hofmeister series or lyotropic sequence, the kosmotropic (structure-maker) versus chaotropic (structure-breaker) properties of ions.[4-10] Many phenomena occurring in condensed phases that involve electrolytes show pronounced ion specificity where different solute molecules exhibit markedly different solvation characteristics.[3, 11-14] The versatility and impact of ion specific effects has been explored in numerous biological and physicochemical processes, *e.g.*, to change the solubility of hydrophobic solutes, to influence the activities of proteins or enzymes, to seed polymerization of aggregates, to tune the thermoresponsive behavior of surfactants, to alter the action of ions on an ion-channel, and to modify the properties of air/water interfaces.[12, 13, 15-21]

As important superchaotropic ions beyond the traditional Hofmeister scale, *closo*-dodecaborate $B_{12}H_{12}^{2-}$ and its halogenated derivatives $B_{12}X_{12}^{2-}$ (X = F−I) and recently attracted considerable attentions due to their potential biomedical applications, for instances, as broadband carriers for peptides membrane translocation and candidates for boron neutron capture therapy and HIV protease inhibitors.[22-25] These borate clusters possess icosahedral symmetry (I_h) with a unique delocalized σ-electron distribution, resulting in high electronic and thermodynamic stability.[5, 26, 27] Replacing H ligands in $B_{12}H_{12}^{2-}$ by cyano groups results in a highly stable $B_{12}(CN)_{12}^{2-}$ dianion with the second electron bound by more than 5 eV (the record in any dianion) and of potential applications as halogen-free electrolytes in ion batteriesries.[28] Furthermore, the derived $B_{12}(CN)_{11}^{-}$ fragment anion shows counterintuitive superelectrophilicity and can bind Ar covalently at room temperature, opening up new directions for activation of inert compounds and elements.[29] Recent studies by us have proved the nucleophilic nature of the H atoms in $B_{12}H_{12}^{2-}$ that enable preferable formation of B–H···H–O dihydrogen bonds (DHBs)[28,29] with water in microsolvation and aqueous environments.[5, 26, 30-32]

Different from the water molecule, acetonitrile (CH_3CN) represents a classic aprotic polar solvent that has been widely used in organic syntheses. Its large dipole

moment (μ = 3.92 D[33]), high dielectric constant, and high capability of dissolving electrolyte salts have stimulated extensive studies on electrolyte-acetonitrile interactions that has evolved into an important subject, particularly, in the fields of electrochemistry and battery applications, where acetonitrile interacts favorably with metal cations via its lone-pair electrons on the nitrile end.[34-37] Similarly, utilizing its negative nitrile group, CH_3CN can act as a weak HB acceptor to form conventional $H_3CCN^{\delta-}\cdots{}^{\delta+}H–X$ hydrogen bonds (HBs).[38] Acetonitrile solvation on anions are less common and under-studied, only a few cases involving halides and pseudo-halides were reported.[39-45] This is largely because the small positive charge is distributed over the three methyl hydrogens in acetonitrile that makes the solvation of anions more intriguing and subtle. The binding motif between an anion X^- and CH_3CN complex is also closely related to the intermediate $X^-\cdots CH_3Y$ in a general nucleophilic S_N2 substitution reaction $X^- + CH_3Y \rightarrow X^-\cdot\cdot CH_3Y \rightarrow XCH_3 + Y^-$.[33, 43, 46-48] Therefore spectroscopic investigation, geometric and energetic characterizations of the intermolecular interactions between anions and the methyl group of acetonitrile could provide important mechanistic insights toward understanding these textbook S_N2 reactions.[42, 44, 49] Previous studies generally suggested that the coordination of an anion with acetonitrile molecule was extremely weak[43] and typically considered via charge-dipole interactions.

Solvating $B_{12}H_{12}^{2-}$ dianions in CH_3CN represents a qualitatively different scenario in the context of anion solvation and posts new challenges/opportunities. The large size of $B_{12}H_{12}^{2-}$ implies less charge density, disfavoring the commonly observed charge-dipole interaction scheme with CH_3CN solvent, while the nucleophilic H atoms in $B_{12}H_{12}^{2-}$ could enable formation of ($B–H^{\delta-}\cdots{}^{\delta+}H–C$) DHB with the methyl group of CH_3CN. Structurally, $B_{12}H_{12}^{2-}$ consists of four boron triangles each with three outward nucleophilic H atoms that could potentially interacts with three electrophilic H on the methyl end; such a combination would heavily favor formation of three ($B–H^{\delta-}\cdots{}^{\delta+}H–C$) DHBs per CH_3CN, *i.e.*, B3–H3 ⋮⋮ H3C–CN. Because CH_3CN has been widely used as a solvent in various dodecaborate salts, it is highly desirable to obtain a molecular-level understanding on the CH_3CN solvating motif and binding strength with $B_{12}H_{12}^{2-}$

from both fundamental and applied science perspectives. Gas-phase negative ion photoelectron spectroscopy (NIPES) coupled with high-level quantum chemical computations has been demonstrated as an ideal and robust technique to obtain the geometric and electronic structure information, and solute-solvent, solvent-solvent interactions for solvated clusters.[12, 50, 51] In this work, we employed this approach to investigate the structural evolution and intermolecular interactions over a series of size-selected acetonitrile-solvated dodecaborate clusters $B_{12}H_{12}^{2-}\cdot n CH_3CN$ (n = 1–4). Our study indicates that each CH_3CN preferably binds to the $B_{12}H_{12}^{2-}$ solute via a B3–H3 ⋮⋮ H3C–CN DHB unit, culminating in forming a highly symmetric tetrahedral cluster of $B_{12}H_{12}^{2-}\cdot 4CH_3CN$, in which all 12 nucleophilic H atoms in the solute are used up to afford 4-fold B3–H3 ⋮⋮ H3C–CN DHB units with 4 evenly-spaced solvent molecules around the solute anion core.

II. METHODS

A. Negative ion photoelectron spectroscopy (NIPES)

The experiments were carried out using a magnetic-bottle NIPES apparatus equipped with an electrospray ionization source (ESI), a quadruple mass spectrometer, a temperature-controlled cryogenic ion trap, and a time-of-flight (TOF) mass spectrometer.[12, 51] The spraying solutions of ~ 1 mM were prepared by dissolving the $K_2[B_{12}H_{12}]$ salt with a mixture solvent of H_2O/CH_3CN with v/v ratio of 1/3. The produced clusters were guided by two RF-only quadruples and directed into the cryogenic Paul trap set at 20 K, where they were accumulated and thermalized for 20–100 ms by collisions with a cold buffer gas (20% H_2 balanced in helium). The cryogenically cooled anions were then pulsed out into the extraction zone of the TOF mass spectrometer for the subsequent mass-to-charge separation. The desired clusters were each selected and maximally decelerated followed by direct photodetachment using 193 nm photons (6.424 eV from an ArF laser). The detached photoelectrons were collected with nearly 100% efficiency by the magnetic bottle and analyzed in a 5.2 m long electron flight tube. The laser was operated at 20 Hz with the ion beam off and on at alternating laser shots, affording shot-to-shot background subtraction. Those

obtained TOF electron spectra were converted to the electron kinetic energy spectra, calibrated with the known spectra of I^- and $OsCl_6^{2-}$.[52, 53] The electron binding energy (EBE) spectra were obtained by subtracting the electron kinetic energy spectra from the detached photon energy. The energy resolution ($\Delta E/E$) was ~2%, *i.e.*, ~20 meV full width at half-maximum (fwhm) for 1 eV kinetic energy electrons.

B. Computational details

The most stable structures of $B_{12}H_{12}^{2-}\cdot n CH_3CN$ (n = 1–4) and $B_{12}X_{12}^{2-}\cdot CH_3CN$ (X = F – I) were obtained using the home-built HydClus code. Firstly, an iterative sampling of initial configurations of clusters was performed with the genmer code,[54] followed by subsequent semi-empirical GFN1-xTB[55] optimizations using the Crest code[56]. Single-point (SP) energy calculations were conducted at the r^{2}SCAN-3c level[57] using the ORCA 5.0.1 software package[58] and thousands of low-energy configurations were selected into the next step according to their energy levels. Secondly, the retained configurations were further optimized at the r^{2}SCAN-3c level, and their SP energies were refined at the ωB97X-2-D3(BJ)[59]/ma-def2-TZVPP level. Dozens of low-lying configurations were selected into the next step accordingly. Finally, geometry optimizations for selected structures were performed at the DFT-B3LYP-D3(BJ)[60]/ma-def2-TZVP[61] level using the Gaussian 16 software[62]. Vibrational frequencies were computed to obtain zero-point energies (ZPEs) and to confirm that they correspond to stationary points on the potential energy surface. The final SP energies were calculated at the post-Hartree-Fock (PHF) DLPNO-CCSD(T)[63]/maug-cc-pVQZ level. In addition, the Shermo code[64] was applied to obtain the corrected Gibbs free energy at 20 K with a scale factor of 0.9860[65] for the ZPE. The vertical detachment energies (VDEs) of $B_{12}H_{12}^{2-}\cdot n CH_3CN$ were calculated using various methods including DLPNO-CCSD(T), IP-EOM-DLPNO-CCSD[66], and PBE0[67], all with the consistent maug-cc-pVTZ basis set. The independent gradient model based on Hirshfeld partition (IGMH),[68] quantum theory of atoms-in-molecules (QTAIM), and restrained electrostatic potential (RESP)[69] charges for each low-energy isomer were generated using the Multiwfn program[70] and rendered using the VMD software[71]. The energy decomposition analysis (EDA) based

on symmetry-adapted perturbation theory (SAPT) at the SAPT2+/aug-cc-pVDZ level was conducted using the PSI4 program[72] to reveal the nature of intermolecular interactions between $B_{12}H_{12}^{2-}$ and acetonitrile molecules. The EDA based on computationally more efficient sSAPT0/jun-cc-pVDZ(-pp) level is also performed for $B_{12}X_{12}^{2-}\cdot CH_3CN$ (X = F – I).

The AIMD simulations based on the B97-3c method[73] were carried out using the ORCA 5.0.1 software to study temperature-dependent dynamic stability of the solvated clusters. The canonical sampling with velocity scaling-reheat was employed to control the temperature, with a time step of 1.0 fs and a time constant of 30 fs. The most stable conformation from each cluster was selected as the initial state, and a 2 ps dynamic trajectory was generated at different temperatures (20, 100, 200, 298, 400, 500, 600, 700, 800, 900, and 1000 K) by randomly initializing atomic velocities according to the corresponding Maxwell distribution at each temperature.

III. RESULTS AND DISCUSSION

Fig.1 shows an overview of the NIPE spectra of $B_{12}H_{12}^{2-}\cdot n CH_3CN$ (n = 0–4) measured at 20 K using 193 nm photons. All spectra exhibit an overall similar broad band with a 2-eV width measured from the baseline albeit with a distinct fine structure for each species. The electron binding energy (EBE) increases monotonically but with different degrees upon each CH_3CN molecule addition, suggesting a stepwise electronic stabilization for the solvated clusters. When the first CH_3CN molecule is attached, $B_{12}H_{12}^{2-}$ exhibits a significant EBE shift (ΔEBE) of 0.41 eV, estimated from the photoelectron signal threshold. Subsequent addition of the solvent continues to increase EBE with a slightly reduced ΔEBE (n) (EBE(n) – EBE(n-1)) values of 0.35, 0.33, and 0.30 eV for n = 2, 3, 4, respectively (Fig.1 and Table 1).

The experimental ΔEBE(n) is intrinsically connected to the stepwise binding energy BE(n) upon the n^{th} solvent attaching to the (n-1) cluster.[12] A notably larger ΔEBE(1) for CH_3CN (0.41 eV) than H_2O (0.31 eV)[30] suggests a stronger binding ability for CH_3CN than H_2O. The ΔEBE(n) slightly decreases with increasing n, 0.35, 0.33, and 0.30 eV for n = 2, 3, and 4, all of them still larger than or nearly the same compared

to the 1st water BE. Thus the NIPES experiments unequivocally indicate unexpected strong interactions between the $B_{12}H_{12}^{2-}$ solute and CH_3CN solvent.

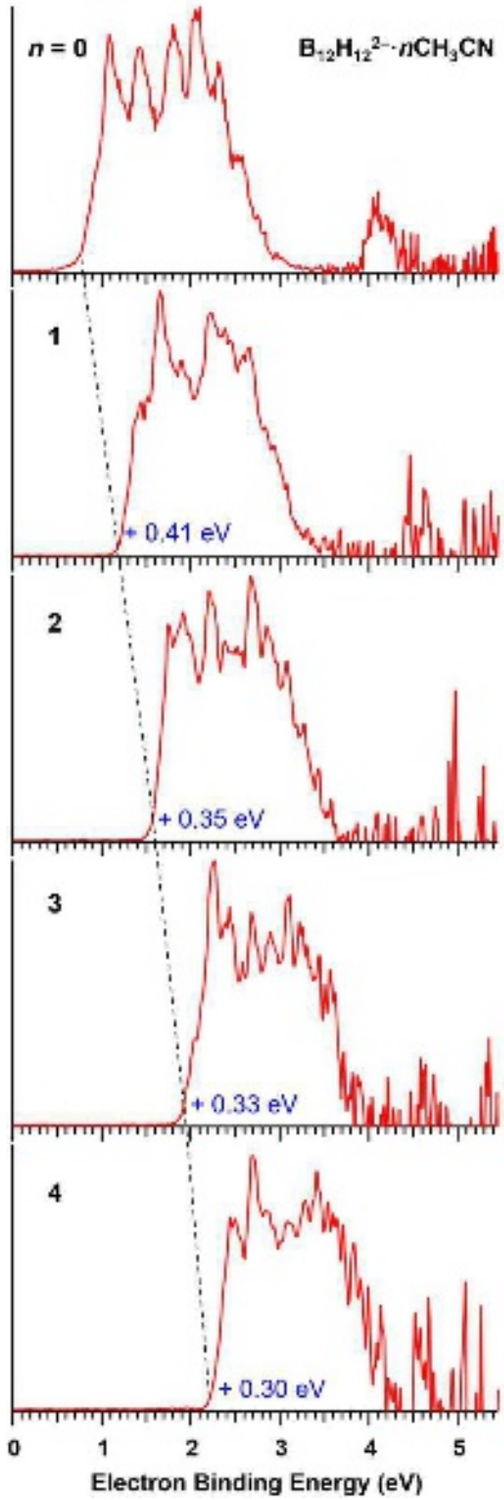

FIG. 1. The 20 K NIPE spectra of $B_{12}H_{12}^{2-}\cdot n CH_3CN$ (n = 0−4) measured with 193 nm photons. The dashed lines indicate the EBE increase trend upon solvation with each stepwise ΔEBE value listed.

TABLE I. Experimental and Calculated VDEs and ΔVDEs (in eV) of $B_{12}H_{12}^{2-}\cdot nCH_3CN$ (n = 0−4).

n	VDE				ΔVDE			
	Expt[a]	Calc[b]			Expt[a]	Calc[b]		
		PBE0	IP-EOM-DLPNO-CCSD	DLPNO-CCSD(T)		PBE0	IP-EOM-DLPNO-CCSD	DLPNO-CCSD(T)
0	1.15	1.27	1.35	1.33	-	-	-	-
1	1.56	1.70	1.71	1.73	0.41	0.43	0.36	0.40
2	1.91	2.11	2.12	2.11	0.35	0.41	0.41	0.38
3	2.24	2.51	2.53	2.49	0.33	0.40	0.41	0.38
4	2.54	2.91	2.93	2.86	0.30	0.40	0.40	0.37
MAE	-	0.22	0.25	0.22	-	0.063	0.073	0.040

[a] Assuming ΔEBE (n) = ΔVDE(n), all experimental VDE(n) values can be estimated by summing up VDE(n-1) and ΔVDE(n) with the VDE = 1.15 eV for $B_{12}H_{12}^{2-}$ derived from ref.[30] The experimental uncertainties are ± 0.05, ± 0.02 eV for VDE and ΔVDE, respectively. [b]All computations were carried out with the maug-cc-pVTZ basis set.

Theoretical calculations were performed to provide crucial information for assigning the cluster structures when combined with the above measured NIPE spectra. Fig. 2 illustrates the B3LYP-D3(BJ)/ma-def2-TZVP lowest-lying structures and their structural evolution. For n =1, the added acetonitrile molecule is bound by forming 3 DHBs in the form of B3–H3 ⋮⋮ H3C–CN between the three adjacent nucleophilic H atoms of $B_{12}H_{12}^{2-}$ and three methyl hydrogens of acetonitrile. For n ≥ 2, distinct binding motifs were observed for CH_3CN compared to the cases in water. Unlike the hydrated $B_{12}H_{12}^{2-}\cdot nH_2O$ clusters in which the added water molecules tend to attach with each other,[31] the added CH_3CN molecules separately occupy different faces of the $B_{12}H_{12}^{2-}$ spherical surface without bearing a tendency of self-aggregation, for example, by forming HBs of acetonitrile themselves ($H_3CCN^{\delta-}\cdots{}^{\delta+}H_3CCN$). For n = 2, the 2nd acetonitrile binds to the boron ball's surface by forming additional B3–H3 ⋮⋮ H3C–CN DHB unit, displaying a V-shaped arrangement. Five low-lying isomers, different with respect to the arrangement of two CH_3CN molecules around the borate core, are identified for $B_{12}H_{12}^{2-}\cdot 2CH_3CN$ (Fig. S1), among which isomer 3 with two CH_3CN

occupying exactly opposite side of the borate core and with an almost linear configuration (D_{3d}) is 0.27 kcal/mol high in energy. Such a binding motif, i.e., forming a B3–H3 ⁝⁝ H3C–CN DHB unit per CH_3CN, continues for n = 3 and 4. Notably, the $B_{12}H_{12}^{2-}\cdot 4CH_3CN$ shows a super-tetrahedral configuration with a T symmetry and zero dipole moment, in which all 12 methyl hydrogens perfectly occupy and interact with the 12 hydrogen atoms of $B_{12}H_{12}^{2-}$.

Based on the above optimized geometries, three methods including PBE0, IP-EOM-DLPNO-CCSD, and DLPNO-CCSD(T) were employed to calculate the VDEs (see Table 1 for VDEs of the lowest isomer 1, and supporting information for the VDEs of all other isomers). The calculations show that all three methods can reproduce the experimental VDE trend, but overestimated the experimental VDEs with the mean absolute errors (MAEs) of 0.22 ~ 0.25 eV. When compared to the experimental ΔVDEs, the MAEs become much smaller between 0.040 to 0.073 eV (TABLE I). Particularly, the PHF DLPNO-CCSD(T) predicts a ΔVDE trend (as a function of n) that is in an excellent parallel with the experimental data (Fig. S3).

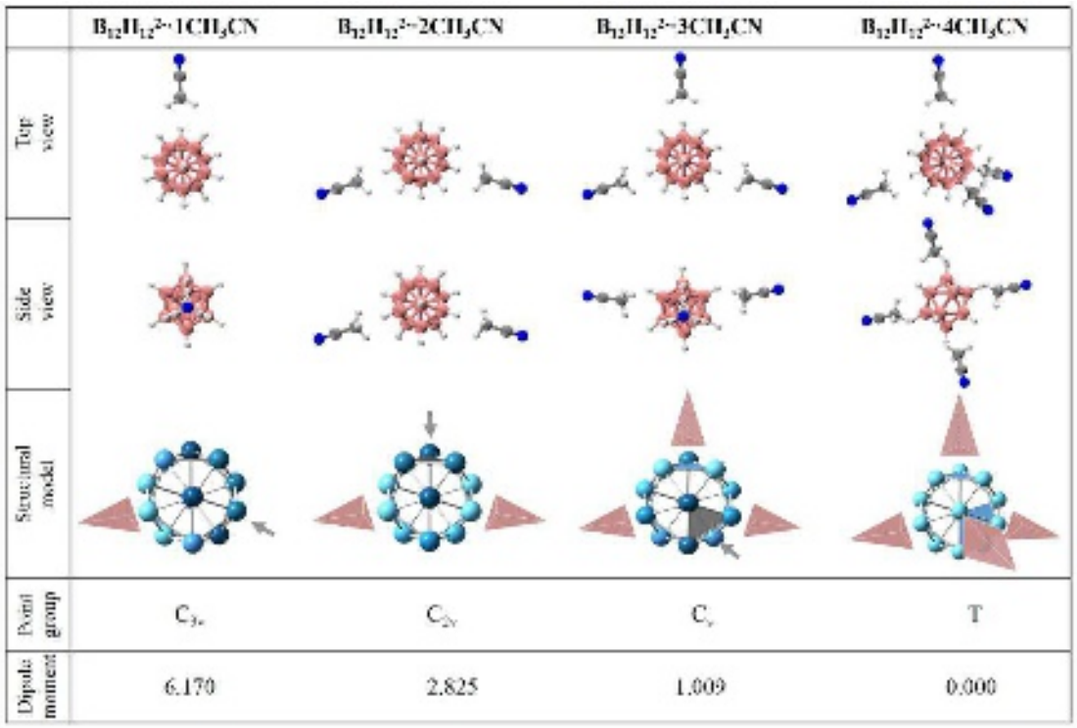

FIG. 2. The lowest-lying structures of $B_{12}H_{12}^{2-}\cdot nCH_3CN$ (n = 1−4) optimized at the B3LYP/ma-def2-TZVP level (see Fig. S1 for other low-lying isomers). The charges of hydrogens on the surface

of $B_{12}H_{12}^{2-}$ are colored from dark blue (most negative) to light blue (least negative). The gray region and the gray arrow suggest the possible potential binding sites for the next CH_3CN. The symmetry (point group) and calculated dipole moment (in Debye) are also listed.

The above structural evolution for $B_{12}H_{12}^{2-}\cdot n CH_3CN$ (n = 1–4) can be rationalized based on the surface charge redistribution of $B_{12}H_{12}^{2-}$ induced by the added CH_3CN molecule (Fig. 2, Fig. S2, and Table S2). The isolated $B_{12}H_{12}^{2-}$ possesses a uniform charge distribution on its molecular surface. As one CH_3CN attached, the surface charges redistribute and the twelve H atoms can be divided into four types: (i) three directly bonded H atoms (light blue) (with the three boron atoms connected to these H atoms labelled as B_{target}); (ii) three unbonded H atoms that connect to those boron atoms each of which links to single B_{target} (dark blue); (iii) three unbonded H atoms linked to the boron atoms each of which connects to two B_{target}; (iv) three unbonded H atoms linked to the boron atoms which have no direct connections with B_{target} (locating exactly opposite side of the borate ball comparing to type i). The calculated RESP charges show that the amount of negative charges carried by the H atoms are in the order of ii > iv > iii > i. Therefore, for n = 2, the potential binding sites on the borate surface for the second CH_3CN is type ii H atoms to form a V-shaped configuration (C_{2v}), not those on the opposite side (type iii). Adding the third or fourth CH_3CN molecule can be explained in a similar way.

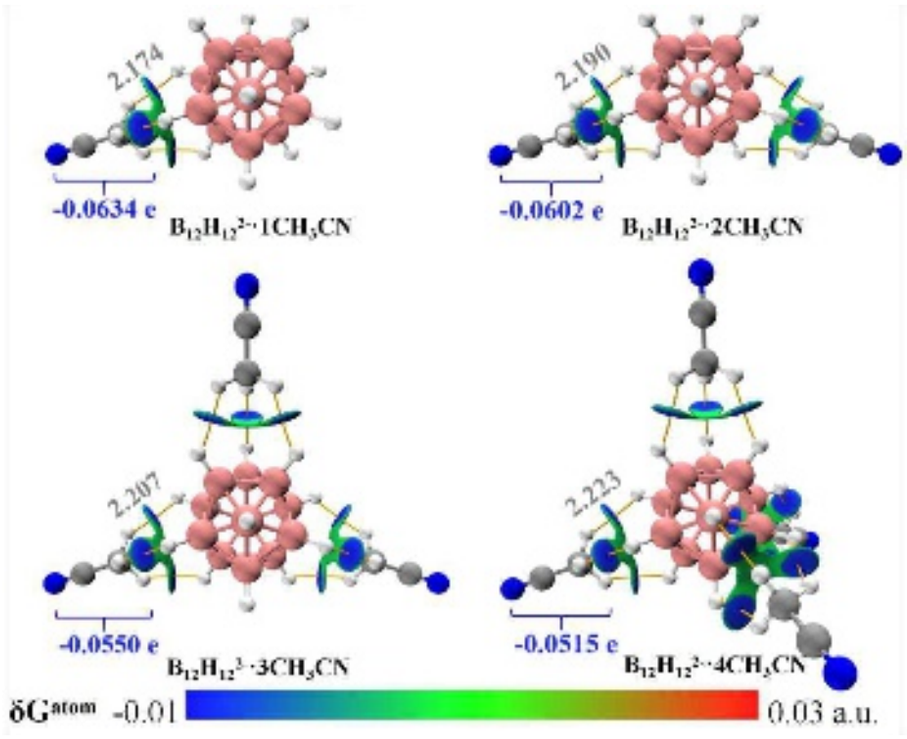

FIG. 3. Analysis of independent gradient model based on IGMH for the lowest-lying structures of $B_{12}H_{12}^{2-}$·$n$$CH_3CN$ (n = 1−4). The δg^{inter} = 0.005 a.u. isosurfaces are colored according to a blue-green-red scheme over a range of -0.01 < sign(λ_2)ρ < 0.03 a.u., where blue represents the strong electrostatic interaction (or HB), green means the weak van der Waals interaction, and red indicates the strong repulsion interaction. The averaged dihydrogen bond lengths (Å) and RESP charges of CH_3CN fragments (e) are also listed.

The Bader's quantum theory of atoms-in-molecules (QTAIM)[74, 75] is employed to reveal the intermolecular interactions and their strengths between $B_{12}H_{12}^{2-}$ and CH_3CN. Within the QTAIM theory, the bond critical point (BCP) is regarded as the most representative point along the interaction path between two interacting atoms.[74] As shown in Table S3, various QTAIM topological descriptors[74, 76-78] such as the electron density $\rho(r)$, Laplacian function of electronic density $\nabla^2\rho$, electronic energy density H(r), potential energy density V(r), Lagrangian kinetic energy density G(r), the ratio of absolute potential energy density to Lagrangian kinetic energy density $|V(r)|/G(r)$ at the BCP of the intermolecular interaction of interest were analyzed. The positive values of $\nabla^2\rho$ and H(r) as well as $|V(r)|/G(r) < 1$ all indicate the existence of noncovalent interactions between the two fragments, visualized intuitively by the blue (strong DHB

interaction) and green regions (weak van der Waals interaction) through independent gradient model based on IGMH analysis[68] (FIG. 3). Interestingly, the values based on these descriptors consistently decrease as *n* increases, suggesting a gradually weakening interaction strength for a single DHB with increasing *n*.

Meanwhile, the total BEs calculated at the SAPT2+/aug-cc-pVDZ level are in line with the experimentally measured blue-shifted VDEs (Table S4a), suggesting that total BEs increase as the cluster size increases. However, when the total BEs are averaged for a single DHB (note there are 3 single DHB per CH_3CN), the averaged BEs are found to gradually decrease as *n* increases. As a result, the averaged SAPT-derived BEs agree well with the QTAIM analysis for characterizing the single DHB strength previously described. Interestingly, a plot of the averaged BE against ρ(r) leads to a perfect linear correlation ($R^2 = 0.99965$), verifying the traditional viewpoint that the larger value of ρ(r), the stronger is the corresponding HB interaction. Moreover, the fitted formula (averaged BE = –349.47ρ(r) – 2.725) provides a very convenient way for evaluating a single DHB strength for other acetonitrile-solvated dodecaborate clusters

The nature of the $B_{12}H_{12}^{2-}$ and CH_3CN intermolecular interactions can be decomposed into four physically meaningful components, including electrostatic (Elst.), exchange (Exch.), induction (Ind.), and dispersion (Disp.) terms. As shown in FIG. 4, the increase of the BE upon each CH_3CN addition arises from the increase of Elst., Ind., and Disp. contributions, in which the first one plays a dominant role although the latter make appreciable contributions. Upon average, the gradual weakening of interaction strength for a single DHB can be attributed to the decreases from both electrostatic and induction terms (FIG. S5). As shown in FIG. 3, the averaged $B–H^{\delta-}\cdots^{\delta+}H–C$ DHB length gradually increases from 2.174 Å (*n* = 1) to 2.223 Å (*n* = 4), suggesting a gradual weakening electrostatic interaction between the two interacting H atoms. The neutral acetonitrile molecules in the meanwhile carry a certain amount of negative charges due to the available induction effect with $B_{12}H_{12}^{2-}$. The induced charges on acetonitrile are found to gradually decrease from -0.0634 e (*n* = 1) to -0.0515 e (*n* = 4), echoing the above decreased induction term based on the SAPT-derived energy decomposition analysis.

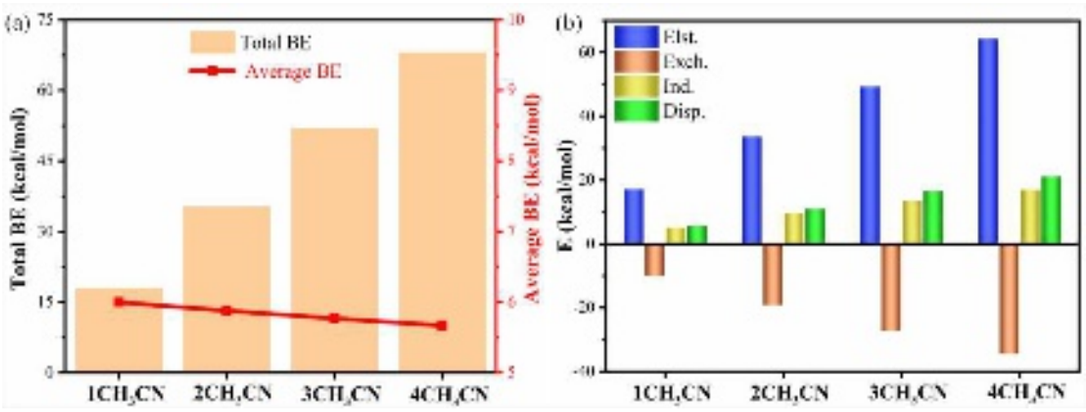

FIG. 4. (a) Calculated binding energies at the SAPT2+/aug-cc-pVDZ level, the red dotted line represents the averaged binding energies corresponding to a single DHB (i.e., divided by 3 per solvent). (b) Electrostatic (Elst.), exchange (Exch.), induction (Ind.), and dispersion (Disp.) terms derived from the SAPT2+/aug-cc-pVDZ energy decomposition analysis for $B_{12}H_{12}^{2-}\cdot n CH_3CN$ (n = 1−4).

To illustrate the dynamic stability of acetonitrile-solvated dodecaborate clusters, temperature-dependent AIMD simulations were conducted for $B_{12}H_{12}^{2-}\cdot CH_3CN$. (FIG. 5). At 20 K, the acetonitrile molecule hardly moves due to the threefold DHB locking between $B_{12}H_{12}^{2-}$ and CH_3CN. As the temperature increases to 400 K, the acetonitrile molecule can still stand on the spherical surface of $B_{12}H_{12}^{2-}$ accompanied with only molecular twisting motions. As the temperature further increases, CH_3CN possesses more freedom and starts to move freely until it detaches from the surface of $B_{12}H_{12}^{2-}$. As a comparison, the water molecule starts to show significant rocking motions even at T = 20 K and be able to swim around the $B_{12}H_{12}^{2-}$ surface at T = 40 K.[30] The temperature-dependent dynamics simulations confirm that $B_{12}H_{12}^{2-}\cdot CH_3CN$ exhibits significant kinetic and thermodynamic stability that can be attributed to the threefold DHB locking force.

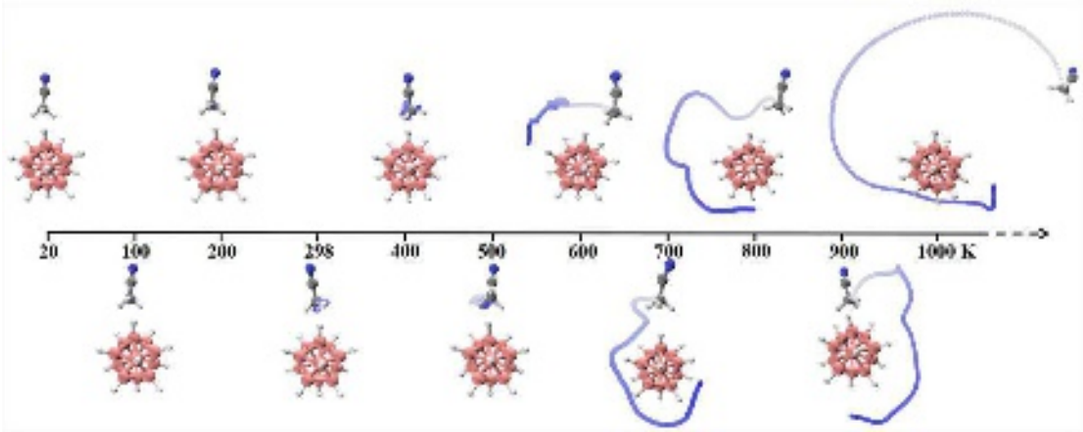

FIG. 5. Simulated trajectories of acetonitrile molecule in $B_{12}H_{12}^{2-}\cdot CH_3CN$ at different temperatures revealed by AIMD simulations. The trajectory tracking is extracted every 10 fs and varies from blue (start) to white (end).

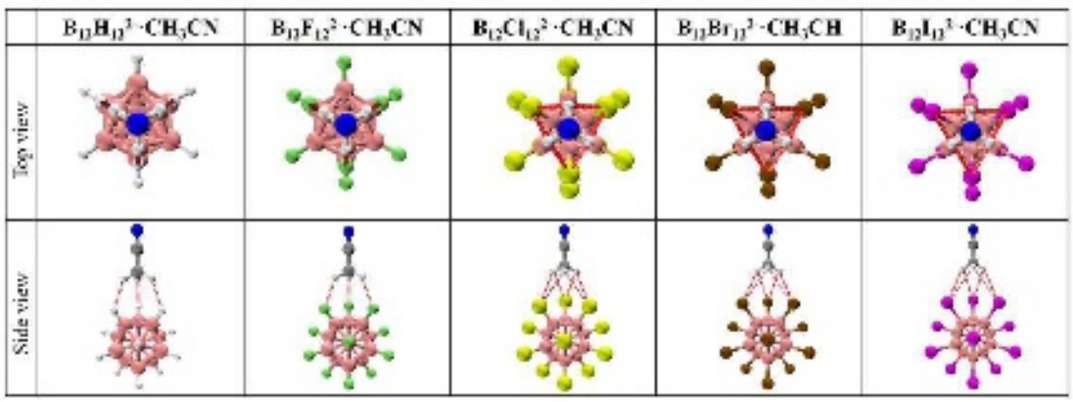

FIG. 6. The lowest-lying structures of $B_{12}X_{12}^{2-}\cdot CH_3CN$ (X = H, F–I).

In addition, the current $B_{12}H_{12}^{2-}\cdot CH_3CN$ model is extended to the whole halogen series of $B_{12}X_{12}^{2-}\cdot CH_3CN$ (X = F – I) (FIG. 6). Compared to $B_{12}H_{12}^{2-}\cdot CH_3CN$, $B_{12}F_{12}^{2-}\cdot CH_3CN$ possesses the same binding motif with three acetonitrile methyl hydrogens directly bound to three adjacent F ligands in the fashion of B3–F3 ⋮ H3C–CN. For $B_{12}X_{12}^{2-}\cdot CH_3CN$ (X = Cl, Br, I), each methyl hydrogen points to the middle of two adjacent halogen atoms with the methyl group rotated by ~60° compared to the H and F cases, a scenario that is similar to what occur in monohydrated $B_{12}X_{12}^{2-}\cdot H_2O$ clusters.[30] Moreover, the EDA for $B_{12}X_{12}^{2-}\cdot CH_3CN$ (X = F – I) are performed at a computationally more efficient sSAPT0/jun-cc-pVDZ(-pp) level (FIG. S6). $B_{12}H_{12}^{2-}\cdot CH_3CN$ possesses a total BE that is 9.5% larger than that for X = F, and 28% lager on average than those of X = Cl, Br, I (Table S5), again illustrating the superiority

of DHB over conventional HBs. The total BE decreases appreciably (by 18%) from F to Cl and converges at Br and I. The EDA results show that the electrostatic and induction interactions gradually decrease with the X size from F to I, while the dispersion interaction increases due to their increased polarizabilities of B-X bonds.[27]

IV. CONLUSIONS

We report a combined NIPES and multiscale theoretical simulation on microsolvation of $B_{12}H_{12}^{2-}$ with 1 to 4 acetonitrile. Each added acetonitrile molecule is found to bind to the solute via a B3–H3 ⁝⁝ H3C–CN DHB motif at the most negative region on the surface of $B_{12}H_{12}^{2-}$. The 3-fold DHBs per solvent leads to significant strength advantage and stable electronic structures. Notably, the $B_{12}H_{12}^{2-}\cdot 4CH_3CN$ cluster displays a super-tetrahedral (T) configuration with zero diploe moment and restores a uniform charge distribution on the surface of *closo*-dodecaborate. The experimental VDEs, particularly the ΔVDEs, are well reproduced by the calculations, lending credence for the most stable structures assigned. In addition, the character and strength of the DHB are characterized by QTAIM and EDA. The averaged BEs for a single DHB decrease as the cluster size increases, attributed to the reduced electrostatic and induction terms. This observation is consistent with an elongated $B–H^{\delta-}\cdots^{\delta+}H–C$ DHB lengths and decreased induced charges on acetonitrile molecules. Temperature-dependent AIMD simulations confirm the extraordinarily kinetic and thermodynamic stabilities based on the $B_{12}H_{12}^{2-}\cdot CH_3CN$ cluster. The binding motif in $B_{12}H_{12}^{2-}\cdot CH_3CN$ is largely retained for the halogenated $B_{12}X_{12}^{2-}\cdot CH_3CN$ (X = F – I) clusters.

This work expands our knowledge on anion-acetonitrile interactions (typically seen as a weak charge-dipole type) and provides direct evidence that multiple DHBs with significant strengths can be formed between $B_{12}H_{12}^{2-}$ and CH_3CN. It appears that the four acetonitrile molecules fully occupy the spherical surface of dodecaborate and whether they truly form its first-solvent shell remains an interesting question and we reserve those issues for subsequent studies.

SUPPLEMENTARY MATERIAL

Five low-lying isomers for each solvated cluster; calculated RESP charges of hydrogen atoms on the surface of *closo*-dodecaborate $B_{12}H_{12}^{2-}$ in $B_{12}H_{12}^{2-}\cdot n CH_3CN$ (n = 1–4); experimental and calculated VDE values and ΔVDEs of the lowest-lying $B_{12}H_{12}^{2-}\cdot n CH_3CN$ (n = 1–4) using various levels of theory. EDA for the lowest-lying structures of $B_{12}X_{12}^{2-}\cdot CH_3CN$ (X = F−I).

ACKNOWLEDGMENTS

The work was supported by the National Natural Science Foundation of China (Nos. 12274128, 12034008, 12250003, and 11727810), Shanghai Rising-Star Program (No. 21QA1402600), and the Program of Introducing Talents of Discipline to Universities 111 Project (B12024). The NIPES work was supported by the U.S. Department of Energy (DOE), Office of Science, Office of Basic Energy Sciences, Division of Chemical Sciences, Geosciences, and Biosciences, Condensed Phase and Interfacial Molecular Science program, FWP 16248. We acknowledge the ECNU Multifunctional Platform for Innovation (001) and HPC Research Computing Team for providing computational and storage resources and the support of NYU-ECNU Center for Computational Chemistry at NYU Shanghai.

AUTHOR DECLARATIONS

Conflict of Interest

The authors have no conflicts to disclose.

Author Contributions

H. S., and X. B. W. designed the research; X. P., W. C., Z. H., Y. Y. and H. S. conducted the research; X. P, H. S., Z. R. S. and X. B. W. analyzed the data; X. P., Z. H., H. S. and X. B. W. wrote the paper. All the authors contributed to the discussions.

DATA AVAILABILITY

The data that support the findings of this study are available from the corresponding author upon reasonable request.

REFERENCES

[1] F. Hofmeister,"Zur Lehre von der Wirkung der Salze," Archiv für experimentelle Pathologie und Pharmakologie **24,** 247-260 (1888).

[2] W. Kunz, J. Henle, and B. W. Ninham,"'Zur Lehre von der Wirkung der Salze' (about the science of the effect of salts): Franz Hofmeister's historical papers," Curr. Opin. Colloid Interface Sci. **9,** 19-37 (2004).

[3] P. Jungwirth, and P. S. Cremer,"Beyond Hofmeister," Nat. Chem. **6,** 261-263 (2014).

[4] K. P. Gregory, G. R. Elliott, H. Robertson, A. Kumar, E. J. Wanless, G. B. Webber, V. S. J. Craig, G. G. Andersson, and A. J. Page,"Understanding specific ion effects and the Hofmeister series," Phys. Chem. Chem. Phys. **24,** 12682-12718 (2022).

[5] K. I. Assaf, and W. M. Nau,"The chaotropic effect as an assembly motif in chemistry," Angew. Chem. Int. Ed. **57,** 13968-13981 (2018).

[6] T. Oncsik, G. Trefalt, M. Borkovec, and I. Szilagyi,"Specific ion effects on particle aggregation induced by monovalent salts within the Hofmeister series," Langmuir **31,** 3799-3807 (2015).

[7] Y. Zhang, and P. S. Cremer,"Interactions between macromolecules and ions: the Hofmeister series," Curr. Opin. Chem. Biol. **10,** 658-663 (2006).

[8] W. Kunz, P. Lo Nostro, and B. W. Ninham,"The present state of affairs with Hofmeister effects," Curr. Opin. Colloid Interface Sci. **9,** 1-18 (2004).

[9] B. Kang, H. Tang, Z. Zhao, and S. Song,"Hofmeister series: insights of ion specificity from amphiphilic assembly and interface property," ACS Omega **5,** 6229-6239 (2020).

[10] H. I. Okur, J. Hladílková, K. B. Rembert, Y. Cho, J. Heyda, J. Dzubiella, P. S. Cremer, and P. Jungwirth,"Beyond the Hofmeister series: ion-specific effects on proteins and their biological functions," J. Phys. Chem. B **121,** 1997-2014 (2017).

[11] K. I. Assaf, and W. M. Nau,"Large anion binding in water," Org. Biomol. Chem. **21,** 6636-6651 (2023).

[12] X.-B. Wang,"Cluster model studies of anion and molecular specificities via electrospray ionization photoelectron spectroscopy," J. Phys. Chem. A **121,** 1389-1401 (2017).

[13] K. D. Collins,"Ions from the Hofmeister series and osmolytes: effects on proteins in solution and in the crystallization process," Methods **34,** 300-311 (2004).

[14] M. D. Baer, and C. J. Mundy,"An ab initio approach to understanding the specific ion effect," Faraday Discuss. **160,** 89-101 (2013).

[15] M. A. Metrick, N. D. C. Ferreira, E. Saijo, A. G. Hughson, A. Kraus, C. Orrú, M. W. Miller, G. Zanusso, B. Ghetti, M. Vendruscolo, and B. Caughey,"Million-fold sensitivity enhancement in proteopathic seed amplification assays for biospecimens by Hofmeister ion comparisons," Proc. Natl. Acad. Sci. **116,** 23029-23039 (2019).

[16] S. Lee, and M. Elimelech,"Salt cleaning of organic-fouled reverse osmosis membranes," Water Res. **41,** 1134-1142 (2007).

[17] K. Xu,"Electrolytes and interphases in Li-ion batteries and beyond," Chem. Rev. **114,** 11503-11618 (2014).

[18] S. Wu, C. Zhu, Z. He, H. Xue, Q. Fan, Y. Song, J. S. Francisco, X. C. Zeng, and J. Wang,"Ion-specific ice recrystallization provides a facile approach for the fabrication of porous materials," Nat. Commun. **8,** 15154 (2017).

[19] V. S. J. Craig, B. W. Ninham, and R. M. Pashley,"Effect of electrolytes on bubble coalescence," Nature **364,** 317-319 (1993).

[20] R. Tian, X. Liu, X. Gao, R. Li, and H. Li,"Observation of specific ion effects in humus aggregation process," Pedosphere **31,** 736-745 (2021).

[21] J. C. Warren, and S. G. Cheatum,"Effect of neutral salts on enzyme activity and structure," Biochemistry **5,** 1702-1707 (1966).

[22] A. Barba-Bon, G. Salluce, I. Lostalé-Seijo, K. I. Assaf, A. Hennig, J. Montenegro, and W. M. Nau,"Boron clusters as broadband membrane carriers," Nature **603,** 637-642 (2022).

[23] J. Warneke, C. Jenne, J. Bernarding, V. A. Azov, and M. Plaumann,"Evidence for an intrinsic binding force between dodecaborate dianions and receptors with hydrophobic binding pockets," Chem. Commun. **52,** 6300-6303 (2016).

[24] K. I. Assaf, M. S. Ural, F. Pan, T. Georgiev, S. Simova, K. Rissanen, D. Gabel, and W. M. Nau,"Water structure recovery in chaotropic anion recognition: high-affinity binding of dodecaborate clusters to γ-cyclodextrin," Angew. Chem. Int. Ed. **54,** 6852-6856 (2015).

[25] P. Cígler, M. Kožíšek, P. Řezáčová, J. Brynda, Z. Otwinowski, J. Pokorná, J. Plešek, B. Grüner, L. Dolečková-Marešová, M. Máša, J. Sedláček, J. Bodem, H.-G. Kräusslich, V. Král, and J. Konvalinka,"From nonpeptide toward noncarbon protease inhibitors: metallacarboranes as specific and potent inhibitors of HIV protease," Proc. Natl. Acad. Sci. **102,** 15394-15399 (2005).

[26] E. Aprà, J. Warneke, S. S. Xantheas, and X.-B. Wang,"A benchmark photoelectron spectroscopic and theoretical study of the electronic stability of $[B_{12}H_{12}]^{2-}$," J. Chem. Phys. **150,** 164306 (2019).

[27] J. Warneke, G.-L. Hou, E. Aprà, C. Jenne, Z. Yang, Z. Qin, K. Kowalski, X.-B. Wang, and S. S. Xantheas,"Electronic structure and stability of $[B_{12}X_{12}]^{2-}$ (X = F-At): a combined photoelectron spectroscopic and theoretical study," J. Am. Chem. Soc. **139,** 14749-14756 (2017).

[28] H. Zhao, J. Zhou, and P. Jena,"Stability of $B_{12}(CN)_{12}^{2-}$: implications for lithium and magnesium ion batteries," Angew. Chem. Int. Ed. **55,** 3704-3708 (2016).

[29] M. Mayer, V. van Lessen, M. Rohdenburg, G.-L. Hou, Z. Yang, R. M. Exner, E. Aprà, V. A. Azov, S. Grabowsky, S. S. Xantheas, K. R. Asmis, X.-B. Wang, C. Jenne, and J. Warneke,"Rational design of an argon-binding superelectrophilic anion," Proc. Natl. Acad. Sci. **116,** 8167-8172 (2019).

[30] Y. Jiang, Q. Yuan, W. Cao, Z. Hu, Y. Yang, C. Zhong, T. Yang, H. Sun, X.-B. Wang, and Z. Sun,"Unraveling hydridic-to-protonic dihydrogen bond predominance in monohydrated dodecaborate clusters," Chem. Sci. **13,** 9855-9860 (2022).

[31] Y. Jiang, Z. Cai, Q. Yuan, W. Cao, Z. Hu, H. Sun, X.-B. Wang, and Z. Sun,"Highly structured water networks in microhydrated dodecaborate clusters," J. Phys. Chem. Lett **13,** 11787-11794 (2022).

[32] K. Karki, D. Gabel, and D. Roccatano,"Structure and dynamics of dodecaborate

clusters in water," Inorg. Chem. **51,** 4894-4896 (2012).

[33] M. Cannon, Y. Liu, L. Suess, and F. B. Dunning,"Dipole-bound CH_3CN^- ions: temperature dependence of ion production rates and lifetimes," J. Chem. Phys. **128,** 244307 (2008).

[34] L. Dongfei, Z. Shuo, Z. Naicui, S. Chenglin, S. He, S. Mingxing, J. Hongsheng, and L. Haibo,"Temperature-dependent study of Fermi resonance of CH_3CN and $CH_3CN\cdots Li^+$ complex in CH_3CN-$LiClO_4$ mixture by Raman spectroscopy," Spectrochim. Acta A **225,** 117507 (2020).

[35] D. M. Seo, P. D. Boyle, O. Borodin, and W. A. Henderson,"Li^+ cation coordination by acetonitrile-insights from crystallography," RSC Advances **2,** 8014-8019 (2012).

[36] D. Seo, O. Borodin, S.-D. Han, Q. Ly, P. D. Boyle, and W. Henderson,"Electrolyte solvation and ionic association. I. acetonitrile-Lithium salt Mixtures: intermediate and highly associated salts," J. Electrochem. Soc. **159,** A553-A565 (2012).

[37] D. M. Seo, O. Borodin, S. D. Han, P. D. Boyle, and W. A. Henderson,"Electrolyte solvation and ionic association II. acetonitrile-Lithium salt mixtures: highly dissociated salts," J. Electrochem. Soc. **159,** A1489 (2012).

[38] J. E. Del Bene,"Hydrogen bonding: methodology and applications to complexes of HF and HCl with HCN and CH_3CN," Int. J. Quantum Chem. **44,** 527-541 (1992).

[39] Q. Yuan, W. Cao, M. Valiev, and X.-B. Wang,"Photoelectron spectroscopy and theoretical study on monosolvated cyanate analogue clusters $ECX^-\cdot Sol$ ($ECX^- = NCSe^-$, $AsCSe^-$, and $AsCS^-$; Sol = H_2O, CH_3CN)," J. Phys. Chem. A **125,** 3928-3935 (2021).

[40] W. R. Fawcett, P. Brooksby, D. Verbovy, I. Bakó, and G. Pálinkás,"Studies of anion solvation in polar aprotic solvents," J. Mol. Liq. **118,** 171-178 (2005).

[41] J. F. Coetzee, and W. R. Sharpe,"Solute-solvent interactions. VII. Proton magnetic resonance and infrared study of ion solvation in dipolar aprotic solvents," J. Solution Chem. **1,** 77-91 (1972).

[42] A. K. Mollner, P. A. Brooksby, J. S. Loring, I. Bako, G. Palinkas, and W. R. Fawcett,"Ion-solvent interactions in acetonitrile solutions of Lithium iodide and tetrabutylammonium iodide," J. Phys. Chem. A **108,** 3344-3349 (2004).

[43] A. M. Erkabaev, T. V. Yaroslavtseva, O. G. Reznitskikh, and O. V. Bushkova,"Solvation of anions in acetonitrile solutions: FTIR and quantum chemical study for Br^-, ClO_4^-, AsF_6^-, and $CF_3SO_3^-$," Spectrochim. Acta A **229,** 117873 (2020).

[44] K. Venkata Ramana, and S. Singh,"Raman spectral studies on interactions of Br^- ions with CD_3 group of acetonitrile, nitromethane and dimethyl sulfoxide," J. Mol. Struct. **194,** 73-82 (1989).

[45] R. Ayala, J. M. Martínez, R. R. Pappalardo, and E. Sánchez Marcos,"Theoretical study of the microsolvation of the bromide anion in water, methanol, and acetonitrile: ion-solvent vs solvent-solvent interactions," J. Phys. Chem. A **104,** 2799-2807 (2000).

[46] Z. Kerekes, D. A. Tasi, and G. Czakó,"S_N2 reactions with an ambident nucleophile: a benchmark ab initio study of the $CN^- + CH_3Y$ [Y = F, Cl, Br, and I] systems," J. Phys. Chem. A **126,** 889-900 (2022).

[47] Q. K. Timerghazin, T.-N. Nguyen, and G. H. Peslherbe,"Asymmetric solvation revisited: the importance of hydrogen bonding in iodide-acetonitrile clusters," J. Chem. Phys. **116,** 6867-6870 (2002).

[48] P. Manikandan, J. Zhang, and W. L. Hase,"Chemical dynamics simulations of $X^- + CH_3Y \rightarrow XCH_3 + Y^-$ gas-phase S_N2 nucleophilic substitution reactions. nonstatistical dynamics and nontraditional reaction mechanisms," J. Phys. Chem. A **116,** 3061-3080 (2012).

[49] C. E. H. Dessent, C. G. Bailey, and M. A. Johnson,"Dipole-bound excited states of the $I^-\cdot CH_3CN$ and $I^-\cdot(CH_3CN)_2$ ion-molecule complexes: evidence for asymmetric solvation," J. Chem. Phys. **103,** 2006-2015 (1995).

[50] X.-B. Wang, X. Yang, J. B. Nicholas, and L.-S. Wang,"Bulk-like features in the photoemission spectra of hydrated doubly charged anion clusters," Science **294,** 1322-1325 (2001).

[51] X.-B. Wang, and L.-S. Wang,"Development of a low-temperature photoelectron spectroscopy instrument using an electrospray ion source and a cryogenically controlled ion trap," Rev. Sci. Instrum. **79,** 073108 (2008).

[52] D. Hanstorp, and M. Gustafsson,"Determination of the electron affinity of iodine," J. Phys. B: At., Mol. Opt. Phys. **25,** 1773 (1992).

[53] X.-B. Wang, and L.-S. Wang,"Photodetachment of free hexahalogenometallate doubly charged anions in the gas phase: $[ML_6]^{2-}$, (M=Re, Os, Ir, Pt; L=Cl and Br)," J. Chem. Phys. **111,** 4497-4509 (1999).

[54] T. Lu, Molclus program, Version 1.12, http://www.keinsci.com/research/molclus.html (accessed Mar 1, 2022).

[55] S. Grimme, C. Bannwarth, and P. Shushkov,"A robust and accurate tight-binding quantum chemical method for structures, vibrational frequencies, and noncovalent interactions of large molecular systems parametrized for all spd-block elements (Z = 1-86)," J. Chem. Theory Comput. **13,** 1989-2009 (2017).

[56] P. Pracht, F. Bohle, and S. Grimme,"Automated exploration of the low-energy chemical space with fast quantum chemical methods," Phys. Chem. Chem. Phys. **22,** 7169-7192 (2020).

[57] S. Grimme, A. Hansen, S. Ehlert, and J.-M. Mewes,"r^2SCAN-3c: a "Swiss army knife" composite electronic-structure method," J. Chem. Phys. **154,** 064103 (2021).

[58] F. Neese,"Software update: the ORCA program system, version 4.0," WIREs Comput. Mol. Sci. **8,** e1327 (2018).

[59] N. Mehta, M. Casanova-Páez, and L. Goerigk,"Semi-empirical or non-empirical double-hybrid density functionals: which are more robust?," Phys. Chem. Chem. Phys. **20,** 23175-23194 (2018).

[60] P. J. Stephens, F. J. Devlin, C. F. Chabalowski, and M. J. Frisch,"Ab initio calculation of vibrational absorption and circular dichroism spectra using density functional force fields," J. Phys. Chem. **98,** 11623-11627 (1994).

[61] J. Zheng, X. Xu, and D. G. Truhlar,"Minimally augmented Karlsruhe basis sets," Theor. Chem. Acc. **128,** 295-305 (2011).

[62] M. J. Frisch, G. W. Trucks, H. B. Schlegel, G. E. Scuseria, M. A. Robb, J. R. Cheeseman, G. Scalmani, V. Barone, G. A. Petersson, H. Nakatsuji, X. Li, M. Caricato, A. V. Marenich, J. Bloino, B. G. Janesko, R. Gomperts, B. Mennucci, H. P. Hratchian, J. V. Ortiz, A. F. Izmaylov, J. L. Sonnenberg, Williams, F. Ding, F. Lipparini, F. Egidi, J. Goings, B. Peng, A. Petrone, T. Henderson, D. Ranasinghe, V. G. Zakrzewski, J. Gao,

N. Rega, G. Zheng, W. Liang, M. Hada, M. Ehara, K. Toyota, R. Fukuda, J. Hasegawa, M. Ishida, T. Nakajima, Y. Honda, O. Kitao, H. Nakai, T. Vreven, K. Throssell, J. A. Montgomery Jr., J. E. Peralta, F. Ogliaro, M. J. Bearpark, J. J. Heyd, E. N. Brothers, K. N. Kudin, V. N. Staroverov, T. A. Keith, R. Kobayashi, J. Normand, K. Raghavachari, A. P. Rendell, J. C. Burant, S. S. Iyengar, J. Tomasi, M. Cossi, J. M. Millam, M. Klene, C. Adamo, R. Cammi, J. W. Ochterski, R. L. Martin, K. Morokuma, O. Farkas, J. B. Foresman, and D. J. Fox, Wallingford, CT, (2016).

[63] C. Riplinger, P. Pinski, U. Becker, E. F. Valeev, and F. Neese,"Sparse maps-a systematic infrastructure for reduced-scaling electronic structure methods. II. Linear scaling domain based pair natural orbital coupled cluster theory," J. Chem. Phys. **144,** 024109 (2016).

[64] T. Lu, and Q. Chen,"Shermo: a general code for calculating molecular thermochemistry properties," Comput. Theor. Chem. **1200,** 113249 (2021).

[65] J. P. Merrick, D. Moran, and L. Radom,"An evaluation of harmonic vibrational frequency scale factors," J. Phys. Chem. A **111,** 11683-11700 (2007).

[66] A. K. Dutta, M. Saitow, C. Riplinger, F. Neese, and R. Izsák,"A near-linear scaling equation of motion coupled cluster method for ionized states," J. Chem. Phys. **148,** 244101 (2018).

[67] C. Adamo, and V. Barone,"Toward reliable density functional methods without adjustable parameters: the PBE0 model," J. Chem. Phys. **110,** 6158-6170 (1999).

[68] T. Lu, and Q. Chen,"Independent gradient model based on Hirshfeld partition: a new method for visual study of interactions in chemical systems," J. Comput. Chem. **43,** 539-555 (2022).

[69] C. I. Bayly, P. Cieplak, W. Cornell, and P. A. Kollman,"A well-behaved electrostatic potential based method using charge restraints for deriving atomic charges: the RESP model," J. Phys. Chem. **97,** 10269-10280 (1993).

[70] T. Lu, and F. Chen,"Multiwfn: a multifunctional wavefunction analyzer," J. Comput. Chem. **33,** 580-592 (2012).

[71] W. Humphrey, A. Dalke, and K. Schulten,"VMD: visual molecular dynamics," J. Mol. Graph. **14,** 33-38 (1996).

[72] R. M. Parrish, L. A. Burns, D. G. A. Smith, A. C. Simmonett, A. E. DePrince, E. G. Hohenstein, U. Bozkaya, A. Y. Sokolov, R. D. Remigio, R. M. Richard, J. F. Gonthier, A. M. James, H. R. McAlexander, A. Kumar, M. Saitow, X. Wang, B. P. Pritchard, P. Verma, H. F. Schaefer, K. Patkowski, R. A. King, E. F. Valeev, F. A. Evangelista, J. M. Turney, T. D. Crawford, and D. Sherrill,"Psi4 1.1: an open-source electronic structure program emphasizing automation, advanced libraries, and interoperability," J. Chem. Theory Comput. **13,** 3185-3197 (2017).

[73] J. G. Brandenburg, C. Bannwarth, A. Hansen, and S. Grimme,"B97-3c: a revised low-cost variant of the B97-D density functional method," J. Chem. Phys. **148,** 064104 (2018).

[74] S. Emamian, T. Lu, H. Kruse, and H. Emamian,"Exploring nature and predicting strength of hydrogen bonds: a correlation analysis between atoms-in-molecules descriptors, binding energies, and energy components of symmetry-adapted perturbation theory," J. Comput. Chem. **40,** 2868-2881 (2019).

[75] R. Bader, Oxford University Press: Oxford, UK (1990).

[76] A. Shahi, and E. Arunan,"Hydrogen bonding, halogen bonding and lithium bonding: an atoms in molecules and natural bond orbital perspective towards conservation of total bond order, inter- and intra-molecular bonding," Phys. Chem. Chem. Phys. **16,** 22935-22952 (2014).

[77] S. J. Grabowski,"What is the covalency of hydrogen bonding?," Chem. Rev. **111,** 2597-2625 (2011).

[78] T. Lu, and S. Manzetti,"Wavefunction and reactivity study of benzo[a]pyrene diol epoxide and its enantiomeric forms," Struct. Chem. **25,** 1521-1533 (2014).